Compact filters in passive silicon photonics using optical ring resonators

Daniel Hutama[1]

***Abstract*— We report on experimental and simulation results pertaining to the filter response of single and cascaded optical ring resonators (ORRs) in silicon photonics (SiP). Using three-dimensional finite-different time-domain simulations, we identify appropriate design parameters for our ORR devices. Using these parameters, we design a layout for experimental verification on a fabricated device. We show that ORRs can be used to implement compact optical notch filters and wavelength-selective switches. In addition, we show that cascaded ORRs, if appropriately designed, can be used to achieve a broadband transmission spectrum in SiP in the 1500-1600 nm range. Using single ORRs, we achieved a 3 dB bandwidth of 0.26 nm, with an FSR of 18.8 nm and an insertion loss of 2.09 dB. Our cascaded ORR device achieved three discrete 3 dB bandwidths concentrated in a 2 nm wavelength range, with an FSR of about 18 nm and an insertion loss of 3.69 dB.**

I. Introduction

Silicon photonics (SiP) is a rapidly evolving field due to its compatibility with existing CMOS fabrication processes, which allows electronic components to be integrated on the same chip as photonic devices. Developments in SiP devices show promise for new applications in several areas, such as sensing, communications, and computing. Such applications often require compact switch and filter components capable of providing large extinction ratios in a desired wavelength range. One way of implementing such devices is using optical ring resonators (ORRs), which provide a more compact and wavelength-selective alternative to larger Mach Zehnder-based devices [1].

This paper is structured as follows: First, we briefly present theoretical insight into the operation of passive ORR devices. We then present three-dimensional finite-difference time-domain (3D FDTD) simulations to identify appropriate design parameters, and to demonstrate the expected thermal behavior of the devices. Following this, we present the fabricated design and discuss the experimental results.

Optical Ring Resonators

Optical ring resonators are formed by a looped optical waveguide, as shown in Figure 1. Light from a nearby straight waveguide couples into the resonator, with the coupling strength determined by several parameters, such as the gap distance, effective index, and wavelength. An ORR is said to be "on resonance" when the propagating wavelength fits an integer number of times inside the optical length of the ring cavity. In other words,

$$\lambda_{\text{res}} = \frac{2\pi R n_{\text{eff}}}{m}, \qquad m \in \mathbb{Z}^+, \tag{1}$$

[1]The Photonic Systems Group, Department of Electrical and Computer Engineering, McGill University, 3480 University St. room 753, Montreal, Quebec H3A 2A7

where R is the radius of the ring and n_{eff} is the effective index of the guided mode. When an input waveguide is placed in close proximity to an ORR, the incoming signal will selectively couple from the waveguide to the resonator, depending on if the wavelength of the signal satisfies the resonance condition of the ORR.

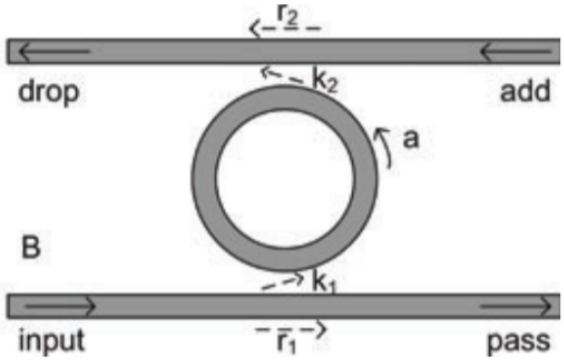

Fig. 1. From [1]. Schematic of an add-drop ring resonator. The self-coupling ratios (r_i) and cross-coupling ratios (k_i) are such that $r_i^2 + k_i^2 = 1$. The dimensions used in this paper are 220 nm x 500 nm for the waveguides, and 5 μm radius for the ring resonators.

Using coupled-mode theory [2], one can find the transmission at the pass and drop ports for the double-bus ring resonator shown in Figure 1:

$$T_p = \frac{r_2^2 a^2 - 2 r_1 r_2 a \cos\phi + r_1^2}{1 - 2 r_1 r_2 a \cos\phi + (r_1 r_2 a)^2} \tag{2}$$

$$T_d = \frac{(1 - r_1^2)(1 - r_2^2) a}{1 - 2 r_1 r_2 a \cos\phi + (r_1 r_2 a)^2}, \tag{3}$$

where ϕ is the single-pass phase shift, given by $\phi = \beta \cdot (2\pi R)$, where β is the propagation constant of the circulating mode. In addition, $a = \exp(-\alpha \cdot 2\pi R/2)$, where α is the power attenuation coefficient $[1/\text{cm}]$.

Under resonant conditions corresponding to $\phi = 2\pi m$, the transmission at the pass port reduces to

$$T_p^{\text{res}} = \frac{(r_2 a - r_1)^2}{(1 - r_1 r_2 a)^2}, \tag{4}$$

with critical coupling occurring for $r_2 a = r_1$, at which point the transmission to the pass port is 0. The double-bus ring resonator can thus act as both a notch filter (at the pass port) and switch (to the drop port) at the resonant wavelength. With this theory in mind, we proceed with simulations to identify the appropriate design parameters to achieve desired coupling.

II. Simulation

Double-bus Resonators

In order to achieve critical coupling, we must identify the appropriate self-coupling and cross-coupling ratios, r_i and k_i, as shown in Figure 1. From equation (4), critical coupling for the double-bus resonator occurs when $r_2 a = r_1$. To simplify our analysis, we assume that the loss is negligible ($a \approx 1$), such that the critical condition is approximately met when the cross-coupling ratios are symmetric, i.e. $|r_1| = |r_2|$ and $|k_1| = |k_2|$. To establish the relationship between gap distance and coupling strength, we performed a series of 3D FDTD simulations, such as the one shown in Figure 2.

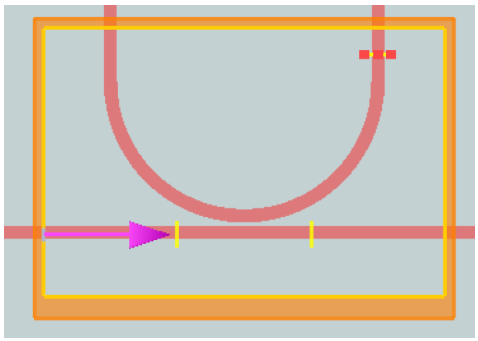

Fig. 2. 3D FDTD setup to identify gap to coupling parameter relationship. Input light is denoted with the magenta arrow. The output at the drop port is measured using a power meter, which measures the power coupling ratio $k = \frac{\frac{1}{2}\int_{\mathcal{S}} \text{real}(\vec{P}) \cdot d\vec{A}}{\text{source power}}$, where $\mathcal{S}$ is the surface of a planar power monitor, $\vec{P}$ is the Poynting vector normal to $\mathcal{S}$, and $d\vec{A}$ is the surface normal element.

The simulated waveguides have cross-section dimensions of 220 nm x 500 nm, which are the same as the fabricated waveguides. The half-ring radius is 5 μm. We performed five simulations, with the parameter of interest being the gap distance. By varying the gap from 100 nm to 200 nm in increments of 25 nm, we observed a Δk of 0.3598, as shown in Table I. As the gap distance decreases, there is a clear trend for an increase in the coupling strength.

TABLE I

Simulated cross-coupling coefficient vs. gap distance.

Gap Distance	k
100 nm	0.7539
125 nm	0.6473
150 nm	0.5583
175 nm	0.4698
200 nm	0.3941

In addition to establishing a relationship between gap distance and coupling strength k, we simulated the spectral response of the double-bus resonator's pass and drop ports. We used an eigenmode solver (Lumerical MODE) to estimate the structure's effective index and loss characteristics. In particular, we found an effective index of 2.445, a group index of 4.062, and a loss of 4.23 dB/cm. We then input the parameters into an optical simulation software (Lumerical INTERCONNECT) to obtain the spectra shown in Figure 3.

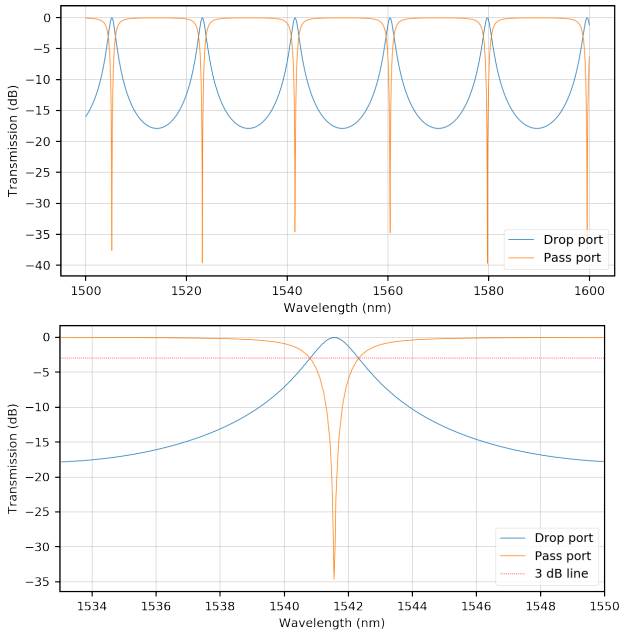

Fig. 3. **Top**: Drop and pass port spectra over the wavelength range of 1500-1600 nm. **Bottom**: Zoom-in of spectra around the resonance at 1541.56 nm.

The simulation results from a symmetric k double-bus resonator suggest a 3 dB bandwidth of about 1.55 nm and a free spectral range (FSR) of 18.8 nm around $\lambda = 1550$ nm. In addition, the simulations suggest large extinction ratios on the pass port (> 30 dB), indicating that the device is close to critically coupled, even when loss is considered ($a \neq 1$). With an attenuation parameter of 4.34 dB/cm, the simulated insertion loss to the drop port is 0.087 dB.

Double-bus Resonator Temperature Dependence

Although not experimentally verified, we simulated the spectral response of the double-bus resonators under different temperatures. As shown in Figure 4, the resonant wavelengths experience a blue-shift of approximately 4.5 nm when the temperature is increased from 270 K to 330 K. As the wavelength shift over this range is larger than the 3 dB bandwidth found in the previous section, we expect that thermal switching will be possible with 5 μm radius rings for the stated temperature variation.

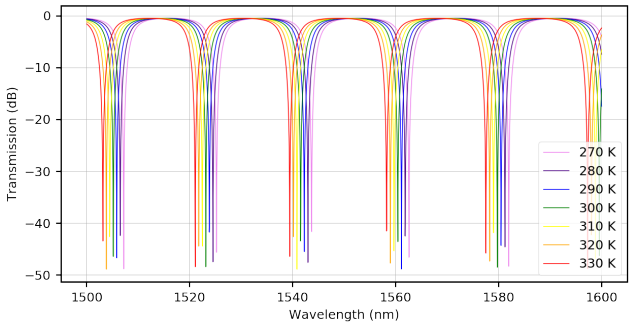

Fig. 4. Simulated pass-port transmission spectrum with temperatures ranging from 270 K to 330 K in increments of 10 K.

Cascaded Resonators

While the drop-port spectrum of the double bus resonator is Lorentzian-like, it may be useful for some applications to have a more flat-top and broadband response. To achieve this, we cascade several rings together, such that the light from the input waveguide couples to the first ring, and subsequently two more before coupling out to the drop port.

We performed simulations on a cascade of three 5-μm ORRs, with the same design parameters as used by Chen *et al.* in their experiment to design a box-like filter [3]. In particular, the gaps were chosen to achieve the following coupling parameters: For the waveguide to the first ring, $k_{wg_1 \to R_1} = 0.5$. From the first ring to the second ring, $k_{R_1 \to R_2} = 0.09$. From the second ring to the third ring, $k_{R_2 \to R_3} = 0.05$. From the third ring to the waveguide, $k_{R_3 \to wg_2} = 0.5$. These coupling parameters approximately correspond to the gap distances of 175 nm, 115 nm, 155 nm, and 175 nm, respectively. Using the coupling parameters, loss characteristics, and effective index information from above, we simulated the cascaded structure in INTERCONNECT, with the results shown in Figure 5.

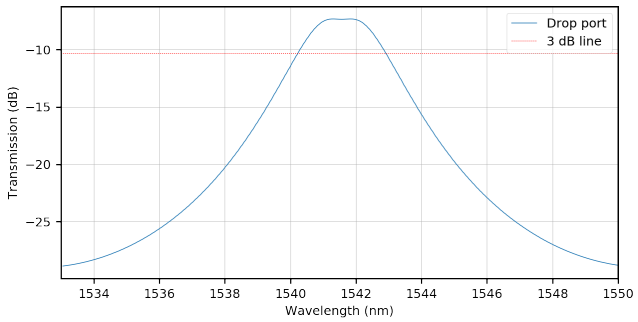

Fig. 5. Simulated drop-port transmission spectrum of the cascaded device, zoomed in on the region around 1541.75 nm.

Our simulation yielded a 3 dB bandwidth of 2.69 nm on the drop port, which is approximately 73.5% larger than the 3 dB bandwidth of the single ring double-bus resonator. The device's insertion loss to the drop port was 7.334 dB. The FSR is approximately 18.42 nm, with an extinction ratio of 21.67 dB around $\lambda = 1550$ nm. Although the extinction ratio experienced noticeable deterioration relative to the single ring double-bus resonator, the 3 dB bandwidth is significantly larger, indicating that the cascaded device can provide a more broadband filter response. As a result, we proceed with the parameters used in simulation for the fabrication and experiment.

III. Experiment

After obtaining the appropriate design parameters from simulation, we designed a layout of the test structures for fabrication, as shown in Figure 6. The layout includes five double-bus ring resonators with varying gap distances. In addition, the there are two cascaded ring resonator structures, with differing gap distances between the outer rings and straight waveguides.

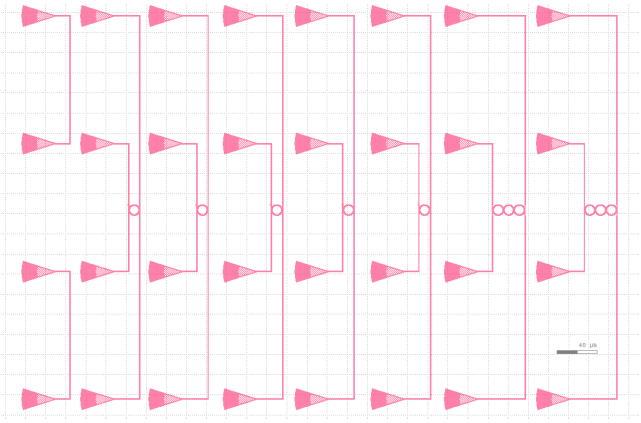

Fig. 6. Device layout submitted for fabrication at Applied Nanotools. From left to right: Loopback structures to isolate grating coupler response. Following this are five 5-μm radius rings with gap distances of 100 nm, 125 nm, 150 nm, 175 nm, and 200 nm. The final two structures are cascaded 5-μm rings. The cascaded structure on the left has gaps of 115 nm and 155 nm, respectively, to the left and right of the middle ring, and a symmetric 175 nm gap from the outer rings to the straight waveguides. The rightmost device is similar, but with 150 nm gaps between the outer rings and waveguides.

Light is coupled in and out of the chip via vertical grating couplers (VGCs) designed for TE mode operation at an incidence angle of $-31°$ [4]. To isolate the spectral response of the VGCs used in the experiment from the response of the test structures, we included two test devices which are simple input-output couplers connected by a strip waveguide. The response of the couplers are averaged, and a fourth order polynomial is used to model the VGC response. The modeled VGC response is then subtracted from the spectral response of all test devices. The adjusted pass and drop spectra for the ring with 100 nm gaps are shown in Figure 7.

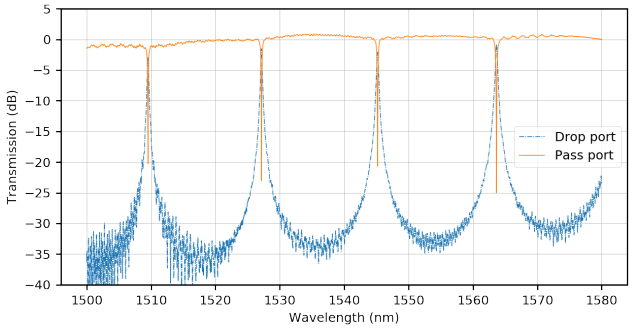

Fig. 7. Drop and pass port transmission spectra for the double-bus ring resonator with 100 nm gaps. The spectral response of the input/output VGCs has been isolated and removed from the graph.

The experimental results exhibit an FSR of 18.44 nm around $\lambda = 1550$ nm, which corresponds to a deviation of less than 2% from the simulated value. An extinction ratio of > 20 dB indicates good coupling, but not quite critical. This is likely due to sidewall roughness contributing to greater losses than anticipated. In addition, manufacturing variability likely had some impact on the gap distances, which consequently impacts k. At the resonance of $\lambda =$

1545.21 nm, shown in Figure 8, the insertion loss to the drop port is 2.09 dB, suggesting that the device is not critically coupled. The 3 dB bandwidth is 0.26 nm, which is sharper than expected from simulation. This is likely due to differences in parameters between simulation and fabrication.

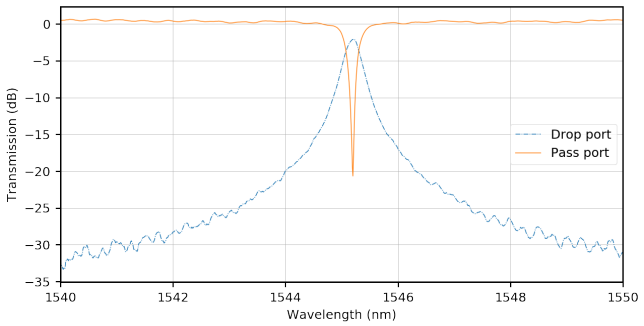

Fig. 8. Zoom-in of drop and pass port transmission spectra for the double-bus ring resonator with 100 nm gaps around the resonance at 1545.21 nm.

The cascaded devices exhibited a best-case insertion loss of 3.69 dB. The FSR is measured at about 18 nm, which is similar to the FSR of the single-ring double-bus resonators. Extinction ratios of around 10 dB indicate that the design is quite far from the critical coupling condition, which is likely due to the increased loss from additional rings. The cascaded resonators fail to provide a continuous 3 dB bandwidth at the drop port, instead providing three discrete 3 dB bandwidths of about 0.25 nm each, as shown in Figure 9 (bottom). However, the three resonance peaks are conjoined, and provide a continuous 1.5 nm 25 dB bandwidth in the range of 1544.2 nm to 1545.7 nm.

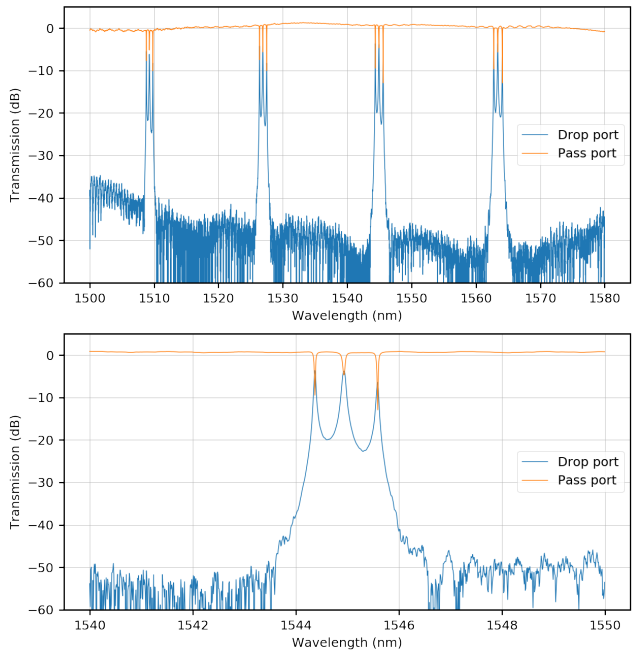

Fig. 9. **Top**: Drop and pass port transmission spectra for the cascaded ring resonator with 150 nm gaps between the straight waveguides and outer rings. **Bottom**: Zoom-in around the resonances in the 1544-1546 nm range.

The fabricated devices exhibited variation in resonance location, likely due to manufacturing variability affecting the optical path length of the ring. The change in optical path length consequently affects the location of the resonances, according to equation (1). The location of the resonances closest to, but less than, $\lambda = 1550$ nm are shown in Table II, where the ring number corresponds to the ordering of rings in the fabricated layout, counting left to right in Figure 6.

TABLE II
RESONANT WAVELENGTHS FOR FABRICATED DEVICES

Ring Number	λ_{res} **[nm]**
1	1455.21
2	1544.38
3	1544.47
4	1544.66
5	1544.70
Average	1544.7 ± 0.3
Simulation	1541.56

As the discrepancy between the experimental and simulation results is statistically significant, it is likely that the simulation parameters do not accurately reflect the fabricated device. Future experiments can work on accurately determining the effective and group indices. In addition, manufacturing variability related to topographical parameters, such as gap distance and ring radius, can be accurately measured using microscopy tools. This will provide circuit designers with a better understanding of the true fabrication output.

IV. CONCLUSION

While our designs have room for improvement, they show the tremendous flexibility of optical ring resonators as switches and notch filters. The presented discrepancies between simulation and experiment can be reduced by implementing an iterative design cycle to better match simulation parameters with fabrication outputs. When combined with active electronics capable of controlling temperature, the strong wavelength selectivity of ring resonators make them strong candidates for implementing wavelength-selective optical switches for DWDM applications. In addition, the sharp drops in transmission spectrum at resonances make ORRs ideal for sensing applications in which environmental changes induce refractive index change, as such changes can be detected as shifts in the resonant wavelength. As the field continues to evolve, optical ring resonators are likely to become increasingly important as compact components capable of executing a variety of functions.

REFERENCES

[1] W. Bogaerts, P. De Heyn, T. Van Vaerenbergh, K. De Vos, S. K. Selvaraja, T. Claes, P. Dumon, P. Bienstman, D. Van Thourhout, and R. Baets, "Silicon microring resonators," *Laser & Photonics Reviews*, vol. 6, no. 1, pp. 46–73, 2012.

[2] S. L. Chuang, *Physics of Photonic Devices*. Wiley, 2009, vol. 2.

[3] P. Chen, S. Chen, X. Guan, Y. Shi, and D. Dai, "High-order microring resonators with bent couplers for a box-like filter response," *Optics Letters*, vol. 39, no. 21, pp. 6304–6307, 2014.

[4] Y. Wang, X. Wang, J. Flueckiger, H. Yun, W. Shi, R. Bojko, N. A. F. Jaeger, and L. Chrostowski, "Focusing sub-wavelength grating couplers with low back reflections for rapid prototyping of silicon photonic circuits," *Optics Express*, vol. 22, no. 17, pp. 20 652–20 662, 2014.